29th AIAA Applied Aerodynamics Conference
27 - 30 June 2011, Honolulu, Hawaii

AIAA 2011-3169

Active Flow Separation Control on a High-Lift Wing-Body Configuration

Part 2: The Pulsed Blowing Application

Vlad Ciobaca[1], Timo Kühn[2] and Ralf Rudnik[3]
German Aerospace Center (DLR), 38108 Braunschweig, Germany

Matthias Bauer[4]
Technical University Berlin (TUB), 10587, Berlin, Germany

and

Burkhard Gölling[5]
Airbus Operations GmbH, Bremen, Germany

This contribution discusses the implementation of active flow separation control for a 3D high-lift wing-body configuration under atmospheric low-speed wind tunnel conditions. The slot-actuators are applied on the suction side of the trailing edge flap to prevent local flow separation. It is the consequent progression of the work presented in Part 1 of this paper. The active flow control (AFC) method of choice is now the pulsed blowing. The experimental results indicate that this AFC technique is feasible for such applications with a global performance enhancement. Here, the wind tunnel findings are briefly discussed while the emphasis is given on the numerical investigations. The verification of the URANS approach points out that the global enhancement through AFC may easily be overestimated by insufficient numerical convergence. Thus, high computational requirements are needed for a consistent numerical evaluation. The computational results highlight the ability of pulsed blowing at moderate blowing momentum coefficients to suppress the flow separation on the trailing edge flap and support the global aerodynamic enhancement. The numerical results show an acceptable agreement with the experimental results for this AFC application.

Nomenclature

AFC	=	Active Flow Control
B-LSWT	=	Low Speed Wind Tunnel at Airbus in Bremen
CFD	=	Computational Fluid Dynamics
CFL	=	Courant Friedrichs Lewy [number]
DLR	=	Deutsches Zentrum für Luft und Raumfahrt [German Aerospace Center]
FFT	=	Fast Fourier Transformation
Iter	=	Number of Computational Iterations
SST	=	Shear Stress Transport [turbulence model]
TUB	=	Technical University Berlin
URANS	=	Unsteady Reynolds Averaged Navier Stokes [method]
A_{ref}	=	Reference Area [m^2]

[1] Research Engineer, Institute of Aerodynamics and Flow Technology, Lilienthalplatz 7.
[2] Research Engineer, Institute of Aerodynamics and Flow Technology, Lilienthalplatz 7.
[3] Head of Transport Aircraft Department, Institute of Aerodynamics and Flow Technology, Lilienthalplatz 7.
[4] Research Assistant, Department of Astronautics and Aeronautics, Marchstrasse 12-14.
[5] Project Supervisor, High-Lift Devices Skill Group, Airbus-Allee 1.

b = Wing Half-Span [m]
C_D = Drag Coefficient [-]
c_{Flap} = Flap Chord Length [-]
C_L = Lift Coefficient [-]
C_p = Pressure Coefficient [-]
C_μ = Blowing Momentum Coefficient [-]
dc = Drag Count [=0.0001] [-]
DC = Actuation Duty Cycle [-]
f = Actuation Frequency [Hz]
F^+ = Dimensionless Frequency [-]
L = Characteristic Length [here, Mean Chord Length] [m]
lc = Lift Count [=0.01] [-]
M = Mach Number [-]
ρ_∞ = Reference Fluid Density [kg/m^3]
Re = Reynolds Number [-]
t = Physical Time [s]
T = Time of One Actuation Cycle [s]
t_{open} = Time of the Open State for One Actuation Cycle [s]
u_{jet} = Jet Velocity [m/s]
U_∞ = Reference Velocity [m/s]
y = Spanwise Coordinate [m]

I. Introduction

THE control of flow separations by active flow control techniques is a promising technology for future transport aircraft. Steep landing approaches and reduced system weights are of significant relevance for any novel high lift design. It is expected that active separation control can lead to a significant reduction of the system complexity in the case of high-lift configurations.

In the past, the need for increasing lift of civil transport aircrafts during landing was countered by increasing the complexity of the high-lift system, e.g. by employing multi-slotted instead of single-slotted flaps[1]. Recent research has proven active flow control (AFC) by means of pulsed blowing from the flap shoulder to be an effective and efficient way to realize the lift requirements. This AFC method forces the flow to stay attached to the flap at flap deflection angles, at which the flow would separate without active intervention. Therefore this technique is promising to enable the design of high-lift systems of reduced mechanical complexity.

Flow control research in Germany has a long tradition at Universities, both theoretical and experimental[2]. Especially for active flap separation control through periodic excitation numerous experimental investigations were carried out in the past at Technical University Berlin (TUB). Tinnap et al.[3, 4, 5] have proven the feasibility of this flow control concept in low Reynolds number, low-speed flows. Petz et al.[6, 7, 8] investigated the influence of excitation parameters on the effectivity of AFC on a 2D configuration consisting of two NACA airfoils and Becker et al.[9] contributed control strategies to these AFC attempts. Such experimental investigations performed in the past suffered from limitations on the used proprietary facilities, which led to limited model sizes, restricted onflow velocities and thus Reynolds numbers, which are too low for a real assessment of flow separation concepts for large transport aircrafts. More recently, in the German Flow Control Network, an experimental test bed and the access to industrial wind tunnel facility was provided by DLR. Haucke et al.[10] and Wild et al.[11] have demonstrated the capability of this AFC strategy – the pulsed blowing through the flap shoulder – to increase the lift of a slatless two-dimensional (2D) high-lift configuration by 50 lift counts at Reynolds numbers of up to 3×10^6.

This article describes the implementation of this active flow control technique on a three-dimensional (3D) civil aircraft half model and discusses first the results obtained for experiments conducted at $M = 0.2$ and $Re = 1.5 \times 10^6$. The emphasis is set afterwards on the numerical simulations of the above mentioned active flow control application.

In contrast to a steady, tangential blowing for the separation control the pulsed blowing is considered to be vastly more energy-efficient, with savings of even one order of magnitude for the blowing momentum coefficient required by a specific performance increment[12, 14]. In the case of periodic excitation large coherent structures are generated, thereby transferring high momentum fluid to the surface, thus being characterized as an unsteady flow.

The numerical simulation of active separation control through periodic excitation still requires experimental data for the validation and the verification of the numerical approaches[13]. Modeling uncertainties (e.g. turbulence models, boundary conditions) are often blamed for poor agreement with the experiment. Nevertheless it was often pointed

out the need for continued high-quality experimentation in this area. For this reason, here the numerical finding will be compared with experimental results where available.

In the followings, the wind tunnel model and the experimental results are briefly discussed. Afterwards the focus is set on the numerical investigations. First, the grid generation and numerical method is presented. Second, the computational results are depicted. Here, a chapter concerning the convergence studies of the URANS simulations is introduced. This resembles the verification for the uniqueness of the solution with respect to the setup of the physical time step size and the inner loop convergence. Only afterwards the performance studies are discussed. Thus, a subsequent chapter is dedicated to the influence of one representative AFC parameter, the blowing momentum coefficient, on the aerodynamic performance for this transport aircraft configuration. Here, local time-averaged flow topologies as well as time-dependent characteristics are presented. In the end the numerical and experimental findings are compared through the lift gain with AFC.

II. Wind Tunnel Model and Experimental Results

A. The wind tunnel model

The experiments described here were conducted using a high-lift wind tunnel model provided by Airbus Operations (Germany) of scale 1:12.7 at the Bremen Low-Speed Wind Tunnel Facility (B-LSWT). This facility's test cross section measures 2.1m x 2.1m. An image of the model mounted in the wind tunnel is provided in Figure 1 (left). Forces and moments are acquired using a six-component balance and are corrected for wind tunnel influences. All tests were conducted at a Mach numbers of $M = 0.2$ and Reynolds numbers of $Re = 1.5x10^6$, respectively. Due to the comparatively low Reynolds number it was necessary to apply transition tripping to ensure *turbulent* flow separation and to avoid laminar separation bubbles. Therefore, a 20µm thick and 1mm wide tape was applied to the leading edges of the flaps.

The high-lift system of this 3D model with a semi-span of 1200mm consists of a slat and a single slotted flap. For the experiments, this model was equipped with an active flow control system, which consists of three major components: a pressurized air supply, fast switching solenoid valves to generate pulsed airflow, and actuator chambers. The jet enters the ambient flow through an orifice in the flap's surface as a fast, pulsed jet. All actuator slots have a constant width of 0.3mm. Their length varies depending on their location in the flap. All actuator slots

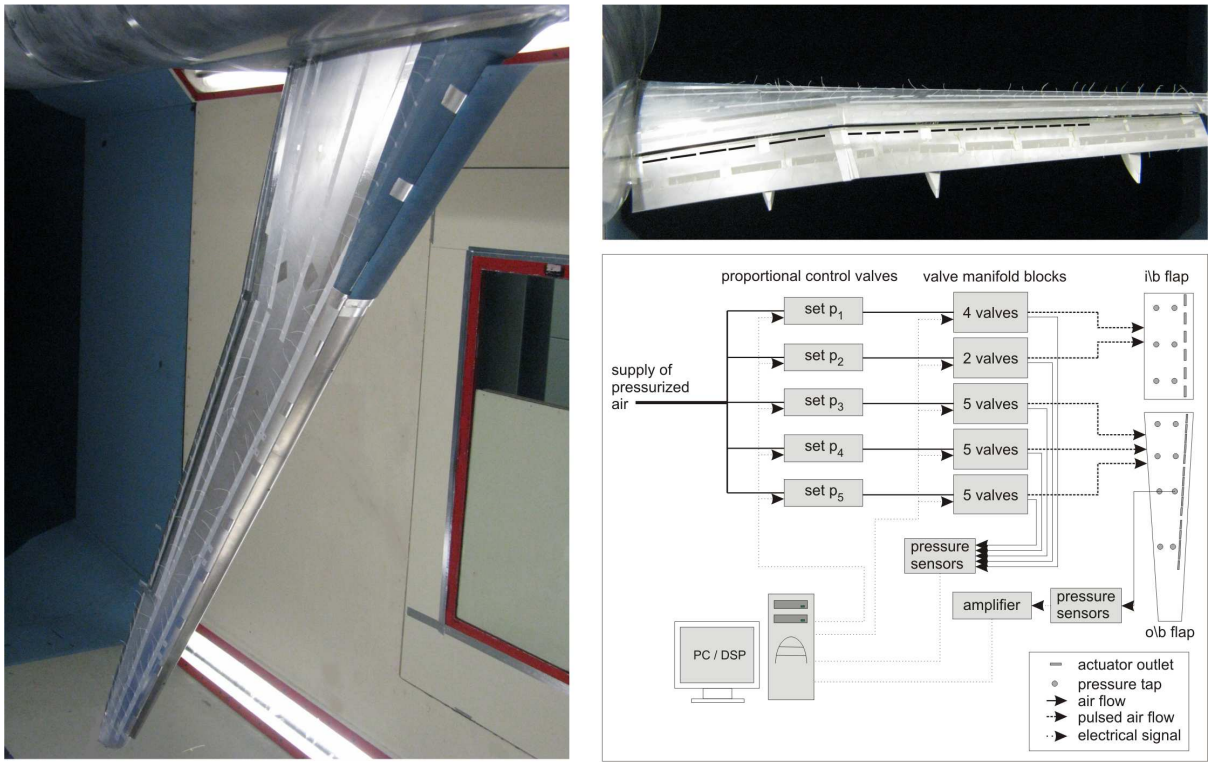

Figure 1. Model owned by Airbus Operations (Germany) in wind tunnel B-LSWT (left); rear view of model with actuator exit slots marked (right, upper side); sketch of the employed actuator system (right, lower side)

are inclined downstream with 30° relative to the flap surface. A total of 21 of those actuator segments are integrated into the flaps and cover approximately 80% of the flap's span. A schematic of the AFC system is sketched in Figure 1 (right). The setup allowed the variation of four important actuation parameters, namely the actuation amplitude, the actuation frequency, the duty cycle of the air pulses, and the phase relation of the jets of neighboring actuator slots.

B. The experimental results

The lift polar for the case when the flow is uncontrolled serves as the baseline for the flow control experiments and is presented in Figure 2 on the left hand side. Here, the flow is largely separated on the flap as can be inferred from the exemplary pressure distribution on the flap provided for an angle of attack close to maximum lift. If active

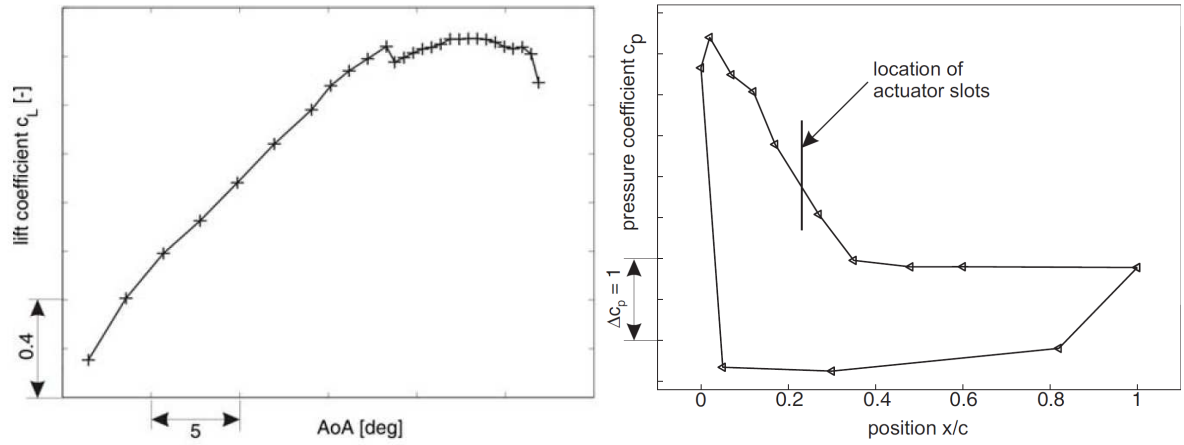

Figure 2. Lift polar without AFC (left); pressure distribution on flap without AFC (right)

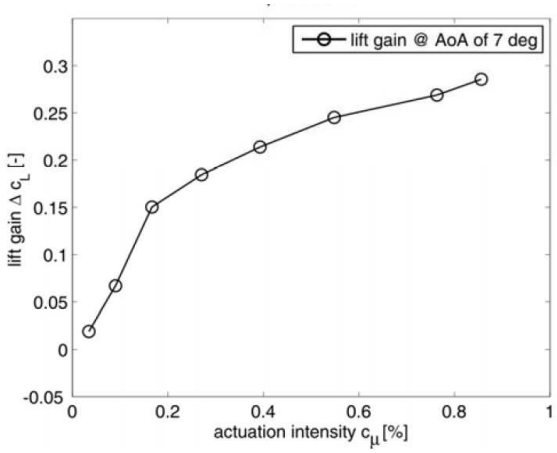

Figure 3. Lift gain for different momentum coefficients

flow control is applied, the flow separation on the flap reduces and the lift of the overall configuration increases. In Figure 3, the lift gain is presented as a function of the momentum coefficient for the actively controlled flow. The other actuation parameters were kept constant at an actuation frequency of 200Hz, a duty cycle of 50%, and all actuators were operated in-phase. Compared to the uncontrolled case, the lift increases by up to 28 lift counts for the maximum momentum coefficient applied. It is noteworthy, that the lift gain does not correlate linearly with the momentum coefficient, but its gradient is reduced for higher values of c_μ.

C. Observations of the System Outputs

In this subchapter some experimental observations are noted for the actuator performance. The results are taken with permission from Bauer et al.[15] and Haucke et al.[10]. The reader is advised that further valuable remarks may be found in these references.

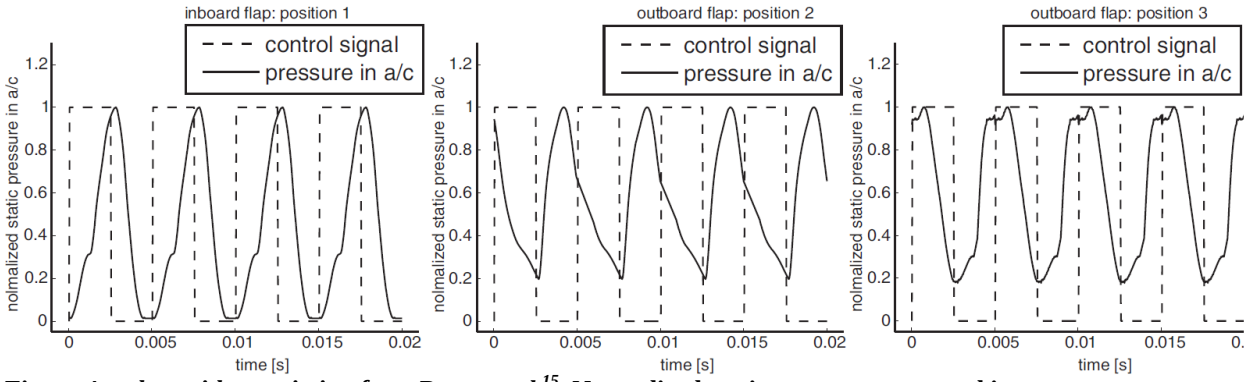

Figure 4. ***taken with permission from Bauer et al.[15]*****. Normalized static pressure measured in one actuator chamber and corresponding electrical control signal from a function generator.**

Figure 4 illustrates results from the same tunnel testing in B-LSWT, for a different flap configuration. It shows the time courses of the static pressure within three actuator chambers, which correlates with the respective jet's exiting velocity. Data is given for a pressure of 8bar applied to the valves working with a duty cycle of DC = 0.5 and a frequency of 200Hz ($C_\mu \approx 0.79\%$). Pressure is normalized with its respective maximum value. It was stated that the originally almost ideal square wave shape of the pressure's time course directly at the exit of the solenoid valves (not shown) has decayed and that there is a phase-shift between the electrical control signal used to drive the valves and the course of the pressure in the chambers. For the present work it is of relevance to notice that the space limitations of the model instrumentation result in deviations of the jet-exit's velocity from the ideal square-shape. Higher accuracy of the pulsed jet-exit's velocity was often achieved as long as the requested space is available in the flap model. One example in this sense is shown in Figure 5, for a 2D high-lift model, where the velocity signal closes the ideal square-shape and during the "closed valve"-stage the velocity falls to zero.

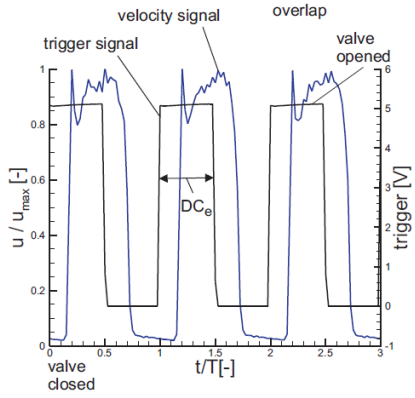

Figure 5. ***taken with permission from Haucke et al.[10]*****. Square wave excitation signal (trigger) vs. time resolved velocity profile in the center of the jet exit without cross flow measured with hot wire.**

III. Grid Generation and Numerical Method

The hybrid grids for the numerical investigations of the pulsed blowing on the trailing edge flap are generated with the mesh generation software CENTAUR[16] and are in-line with the finding of the mesh refinement study conducted for the baseline flow in part 1 of this paper. For the approximation of the boundary layer, there are 30 prism layers with a target y^+-value of 1.0 ensuring an appropriate resolution of the viscous sublayer. As reported in Part 1 portions of the slot-actuators are modeled and the point number of the grid amounts *30 x10*^{6} points, about *5 x10*^{6} points increase compared to the baseline mesh (without slot-actuators). Each modeled actuator increases the mesh size with roughly 250000 points. Figure 6 depicts a 2D-cut for the volume mesh at one actuation's station. For the modeled actuator-slots also a hybrid meshing approach is used with thin prism layers in order to discretize the local boundary layer.

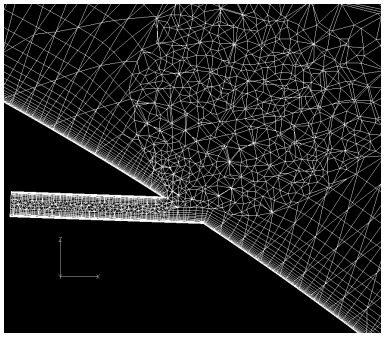

Figure 6. Mesh topology at the actuator-slot

The flow solver used is the finite volume compressible solver TAU developed at the German Aerospace Center (DLR)[17]. A second order central scheme is the method of choice for the discretization of the convective fluxes. The artificial dissipation

based upon the original settings of Jameson is applied with a 2nd order dissipation term of 1/2, and a 4th order dissipation coefficient of 1/64. The URANS simulations are conducted with a dual time stepping approach. Dual time is an alternative means for computations of unsteady flow problems. The time derivate of the considered governing equations is discretized with backward difference formulae, and the resulting algebraic system is solved by iterating to a steady state in an artificially introduced pseudo time. The inner iteration strongly resembles the iteration for convergence to steady state, so that the techniques applied for efficient steady state convergence (see in Part 1) may be applied.

Concerning the turbulence modeling the advanced Shear Stress Transport model (SST) from Menter[18] is applied with a different wall limiter type for the ω-equation, where the lower bound of ω is limited[19] based on experimental assumptions for the wall roughness.

The actuation boundary condition, at the slot's bottom, is of particular interest here. For an inflow boundary condition of three-dimensional subsonic flow, according to the characteristic[20] theory four quantities need to be specified by boundary values and the fifth condition is taken from the solution inside the flow domain. Here, we prescribe the conservative variables for density and momentum and use the value of the pressure from the solution inside the domain. This approach for AFC simulations was previously applied for single actuators on a zero-pressure gradient flat plate[21] and for a slot-actuator on a trailing edge flap of 2D high-lift airfoils[22] as part of the verification and validation process. Here, for the pulsed blowing application the jet velocity changes over time with a square shape signal. The jet velocity at the inflow boundary condition is defined as

$$u_{jet}(t) = u_{jet,\max} \times I_{[0,t_{DC}]}(t_{offset})$$

where $I_{[t_a,t_b]}(t) = 1$ if $t \in [t_a, t_b]$ and zero otherwise.

In order to avoid a sharp jump from 0 to 1, a smoothing method is applied. A time is introduced over which u_{jet} is increased from 0 to its maximum value. The user defined time for smoothing the pulsed signal is typically two orders of magnitudes lower as the time of an actuation cycle. The modeling of parts of the actuator-slots is considered a necessity, where the formulation of the inflow boundary conditions ensures an accurate mass flow. Moreover, the inclusion of actuator-slots is the only possibility to ensure a correct outflow direction.

In order to have a close relation to the wind tunnel tests, the setup is initialized with the Mach number, the Reynolds number, the corresponding reference length of the model and the farfield temperature. The Reynolds number of the wind tunnel experiment is $1.5x10^6$ and the Mach number is 0.2, whereas the farfield temperature is 300K. Based on the results of the wind tunnel campaign, an angle of attack of $\alpha=7^o$ in the linear regime of the lift curve has been selected for the present study.

In order to have an evaluation of the performance improvements of the active flow separation control it is requested to asses the performance without AFC also by the numerical method. A systematic comparison for the mesh refinement and turbulence model studies has guided us to the Menter SST eddy viscosity turbulence model, and to a so called intermediate mesh in terms of the grid refinement study. The impacts due to the inclusion of slot-actuators in the computational domain and due to the new unsteady numerical approach have already been discussed in comparison to the RANS baseline results (see part 1 of this paper).

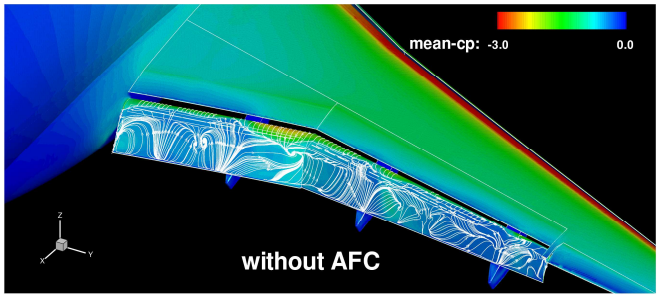

Figure 7. Reference flow topology without AFC (part 1 of this paper)

For the sake of brevity we just recall the flow topology without AFC as reference for simulations with active flow separation control. Figure 7 depicts the average surface pressure and the surface streamlines for the trailing edge flap. It is the target of this AFC application to reduce or suppress the flap separation for a global performance enhancement.

IV. Computational Convergence Studies with AFC

For the URANS simulations the choice of the physical time step size and the convergence in the inner loop play an important role in the verification of the numerical setup for the AFC simulation. A systematic comparison of different magnitudes for the physical time step and the number of iterations in the inner loop stays in focus for this

work. The number of physical time steps is varied between 50 and 400 for one actuation cycle at a constant actuation frequency. For a constant time step size (at 200 time steps per actuation cycle) the number of inner computational iterations is varied in between 25 and 250 and corresponds to a convergence of the aerodynamic coefficients of the order of 10^{-6} up to 10^{-9}.

In order to decide on the most suitable numerical approach for the selected grid and turbulence model the impact of the two parameters mentioned above is analyzed step by step in the next chapters. The flow control setup is fixed for this convergence study at: blowing momentum coefficient $C_\mu \approx 0.1\%$, frequency $F^+=1$, and duty cycle DC=0.5.

At this point we inject a comment on the definition of the relevant quantities for the AFC application. In the experiments the blowing momentum is defined as

$$C_\mu = \frac{\dot{m}_{jet} \times u_{jet}}{\frac{1}{2} \times \rho_\infty \times U_\infty^2 \times A_{ref}}$$

where the jet velocity u_{jet} is typically obtained from conditions before or inside the plenum combined with isentropic flow relations. Unfortunately this methodology introduces some uncertainties. This error source might be suppressed only by field measurements (with cross-flow) at the jet-exit plane including velocity and turbulence quantities. As flowfield data are not available for this complex experimental setup we accept the classical assumptions used to evaluate the jet velocity. Further relevant parameters for the pulsed blowing application are the frequency and the duty cycle. These are defined as

$$F^+ = \frac{f \times L}{U_\infty} \text{ and } DC = \frac{t_{open}}{T}$$

A. Time step size requirements

Figure 8 depicts the lift evolution over time for four values of the physical time step. All computations are started from a previous quasi-converged steady state solution with continuous blowing and are performed with 50 inner iterations for each computed time step. A common approach for the URANS simulations is to select the time step size $\Delta t \sim 0.01xT$, where T is computed based on a reference length and a reference inflow speed. Thus, with the c_{Flap} and U_∞ as references, Δt is of the order of $10^{-4}s$. The selected computational time steps are $10x\,10^{-5}s$, $5x10^{-5}s$, $2.5x10^{-5}s$ and $1.25x10^{-5}s$ for a discretization of each actuation cycle with *50, 100, 200* and *400* time steps, respectively. The lift evolution over time indicates discrepancies between different time step sizes. For the comparison of the mean solutions with different setups the averaging should be performed for the same time interval. More, this time interval should be large enough to assure that additional time will not change the resulting mean values. Figure 8 shows that depending on the time step size different global computational times are needed before averaging a solution are meaningful. For consistency, the comparison of the different solutions is further performed only for half of the total computational time, the last 16 actuation cycles (last 0.08s).

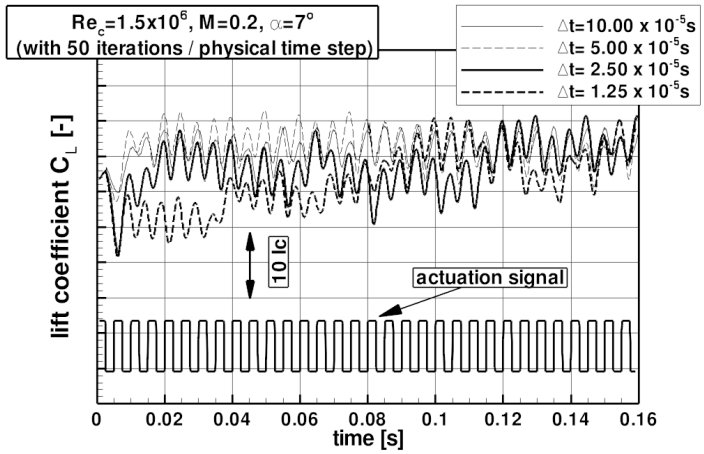

Figure 8. Lift coefficient evolution over time for different physical time step sizes

The mean averaged lift coefficient C_L and drag coefficient C_D shown in Figure 9 indicate maximum changes of the order of *0.02* for C_L and *0.004* for C_D; the smaller the size of the time step the lower is the error in comparison to the corresponding magnitudes at $\Delta t \rightarrow 0$ suggested by general fit curves. The maximum relative error of the aerodynamic coefficients is 1.2% for lift and 2% for drag respectively. The deviations are minor for a complex high lift configuration with large portions of flow separation.

The mean aerodynamic values are not the only indicators for the convergence requirements of the unsteady simulations with AFC. Details of the lift coefficient evolution in time given by a fast Fourier transformation are shown in Figure 10. The highest amplitude is located at the actuation frequency, f=200Hz. With the last three time step magnitudes $\Delta t \leq 5x10^{-5}s$ the flow response on the pulsed blowing application shows similar amplitudes at 200Hz. For the largest time step $\Delta t = 10x10^{-5}s$ an obvious lower amplitude is computed at the actuation frequency. We observe also noticeable discrepancies for the very low frequencies. These are expected as the FFT analysis is conducted for the same time interval, while different time step sizes result in different resolutions for the FFT results. Nevertheless, it is obvious that flow fluctuations at low frequencies still exist for this AFC setup and might be triggered by different local flow separations.

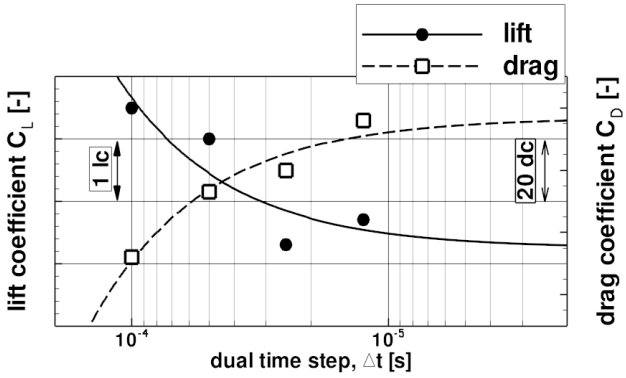

Figure 9. Time-averaged lift- and drag- coefficient at different physical time step sizes

In order to verify the presence of flow separations and quantify the resulting flow topologies the time-averaged surface pressure and average flap's surface streamlines are depicted in Figure 11. Obviously higher suction peaks and reduced flow separations are computed in comparison to the results without AFC (see chapter IV). Nevertheless, the flap flow separation is not fully suppressed by AFC. Where no actuators are implemented (near flap track fairings, and at the end of the outboard flap), the flow topology is mostly unchanged compared to the setup without AFC. A higher blowing momentum coefficient than applied here ($C_\mu \approx 0.1\%$) could further reduce the flap separation. It is interesting to observe that from all 4 graphs only at the largest time step the separation line is located further upstream in comparison to the others. Except minor deviations (suction peak level for the outboard flap) the results for all time steps $\Delta t \leq 5x10^{-5}s$ agree well with each other.

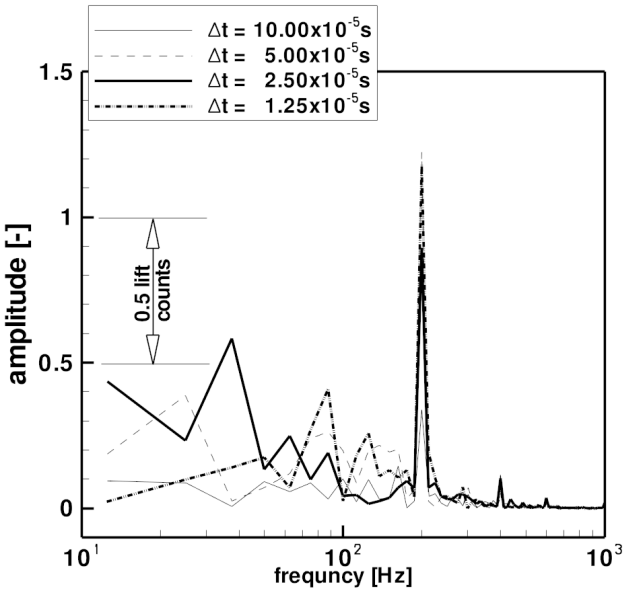

Figure 10. FFT analysis for the time dependent lift coefficient for different physical time step sizes

The importance of the convergence requirements for an unsteady simulation with AFC is made evident in Table 1 by the computational times spent for each of the setups discussed above. It is obvious that the computational time increases linearly with the decrease of the time step magnitude. The smallest time step requests one month of computing with 256 processors on a high performance cluster.

The unsteady computations with pulsed blowing on the flap for active separation control require a time step size $\Delta t \leq 5x10^{-5}s$ for the discussed setup. This corresponds to Δt with values less than a precent of the time of one-actuation-cycle. Thus, more than *100* time steps need to be resolved for each actuation cycle. In order to increase the safety for the other actuation setups (e.g. different blowing momentum coefficients) for the next simulations we selected the $\Delta t = 2.5x10^{-5}s$, *200* time steps for one actuation cycle.

Δt[x10-5s]	CPUh (x10^3)	time on 256 CPUs
10	25	4 days
5	50	8 days
2.5	100	16 days
1.25	200	1 month

Table 1. Computational time spendings

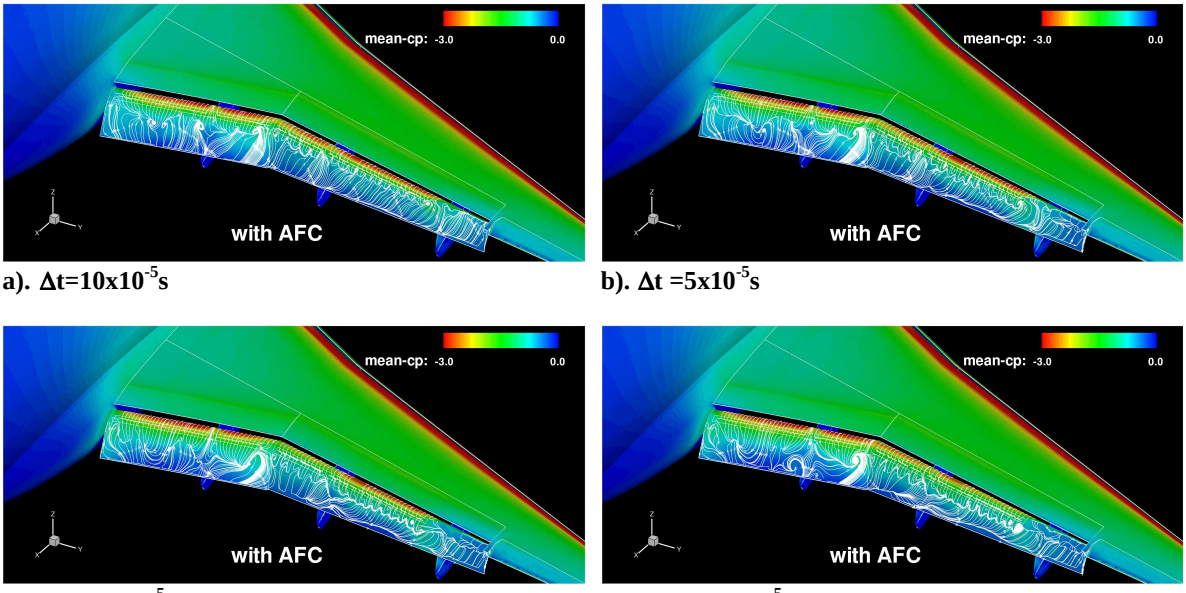

a). $\Delta t=10x10^{-5}s$ b). $\Delta t =5x10^{-5}s$

c). $\Delta t=2.5x10^{-5}s$ d). $\Delta t =1.25x10^{-5}s$

Figure 11. Flow topology with one AFC setup for different physical time step sizes

B. Inner loop convergence requirements

In order to analyze the impact of the convergence level in the inner loop four numerical setups have been selected, with *25*, *50*, *125* and *250* inner iterations for each physical time step $\Delta t=2.5x10^{-5}s$. Figure 12 depicts the resulting lift coefficients over time. In comparison to the time step size variation (Figure 8) now the various curves do not show significant discrepancies for the first actuation cycles. Yet, the solution is not independent of the convergence level with respect to each setup. A look in the convergence characteristics for each time step is shown in Figure 13 for the setup with *250* inner iterations. Here, the density residuum decreases 2 orders of magnitude, while the lift- and drag- coefficient residuum are below 10^{-9}. The levels of convergence at the other three setups are indicated in the same figure. The highest average residuum level for the aerodynamic coefficients is of the order 10^{-6} and corresponds to 25 iterations in the inner loop.

Figure 14 depicts the time-averaged lift and drag results over the mean convergence level of the aerodynamic coefficients in the inner loop. The maximum changes are of the order of *0.03* for C_L and *0.004* for C_D; the better the solution is converged at each time step the lower is the error in comparison to the corresponding magnitudes at $\varepsilon \rightarrow 0$ suggested by general fit curves. The

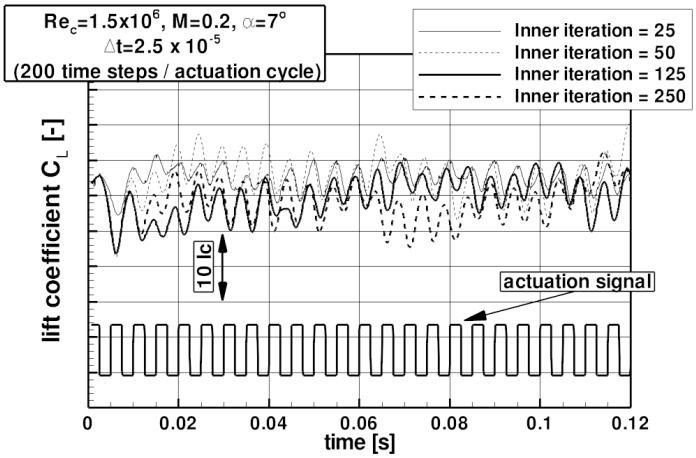

Figure 12. Lift coefficient evolution over time for different inner loop convergence

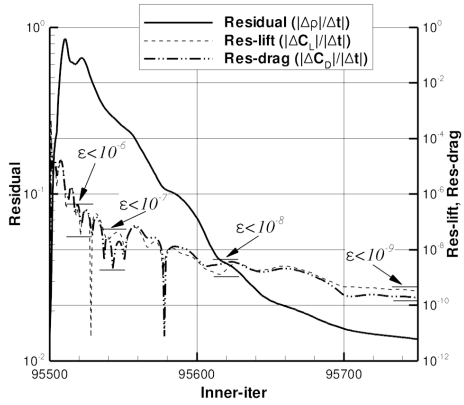

Figure 13. Density, lift and drag residuum for one dual time step (in the inner loop).

maximum error is considered acceptable for a complex high-lift configuration, less than 2% for lift and drag. In order to assure errors smaller than 1%, it is requested to have a minimum convergence level of $5x10^{-8}$, with at least 75 inner iterations.

The fast Fourier transformation of the lift evolution in time is now exemplified for two time intervals in Figure 15. Both analyses exclude the first 4 actuation cycles. The first graph covers 20, while the second graph only the last 8 actuation cycles, respectively. The amplitude at the actuation frequency, f=200Hz, is similar in

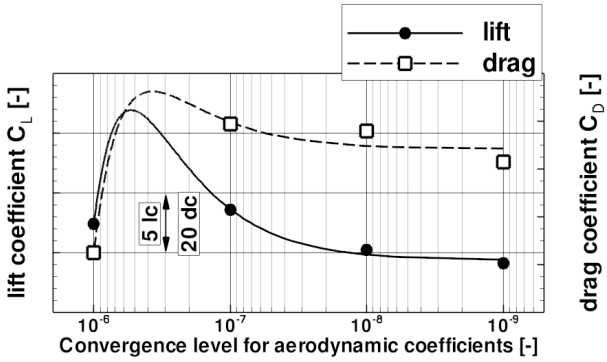

Figure 14. Time-averaged lift- and drag- coefficient at

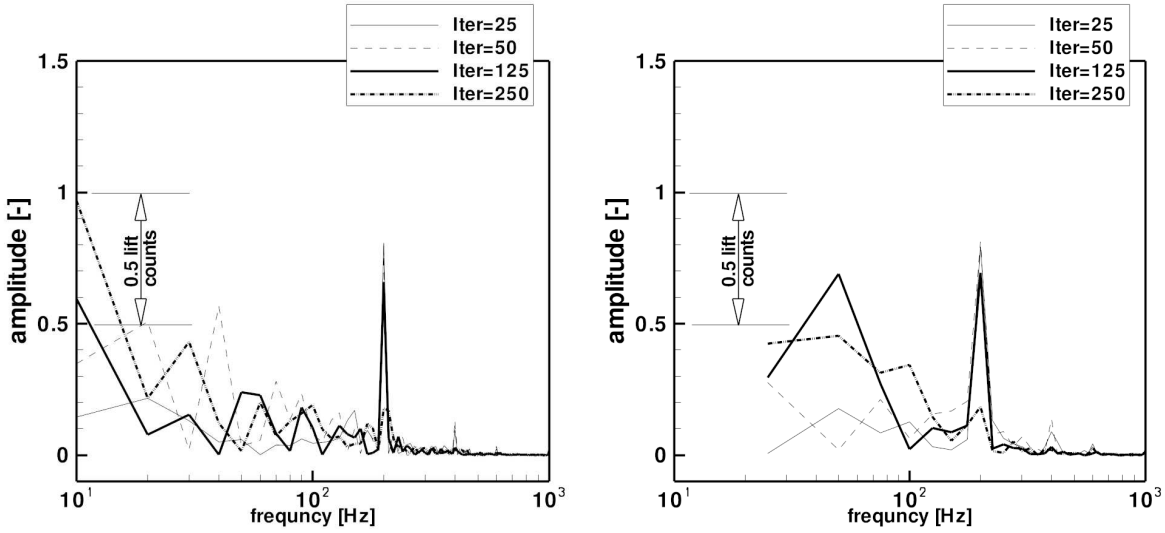

a). t in [0.2, 0.12] **b). t in [0.8, 0.12]**

Figure 15. FFT analysis for the lift coefficient at various numbers of inner iterations

between the two diagrams for each of the four numerical setups. This assures a meaningful averaging of the solution for only the last 0.04s. It is evident that for the best inner loop convergence (*Iter=250*) the amplitude at f=200Hz is lower as for the other three setups, and high amplitudes are computed for lower frequencies. Here, the flow is dominated by large coherent structures at lower frequency as the one used by the actuation system.

With the confidence that a time averaging for a time interval of the last 0.04s is representative, the resulting mean flow topologies are now shown in Figure 16 by average surface pressure and average surface streamlines on the trailing edge flap. With respect to the mean separation line the single outlier is the result with the smallest number of inner iterations, *Iter=25*, while the other mean solutions match well with each other. Beside the local surface streamlines, the pressure distributions point towards higher suctions peaks for the outboard flap when the solution is less converged in the inner loop. While the local flow in the outboard flap region reveals that high number of inner iterations is requested for a good convergence, at the inboard flap there are no differences for the computations with Iter≥50.

It is evident that the larger the number of inner iterations the higher is the requested number of CPUh for the numerical evaluation. Here, for the setup *Iter=250*, the computational time on 256 CPUs is of the order of 80 days on a high performance cluster.

We conclude that with the present solver setup, a minimum requirement for the URANS computations with AFC is to achieve a residuum level for each time step of $5x10^{-8}$ for the aerodynamic coefficients. In order to assure the consistency for more than one AFC setup we proceed further with a fixed number of inner iterations, *Iter=125*, which corresponds to lift residuum levels of $1x10^{-8}$ for the above discussed test case, $C_\mu \approx 0.1\%$.

The convergence study for the URANS simulations with active flow separation control shows that the addition of large physical time steps and low number of inner iterations results in higher computed lift for the complex high-lift wing body configuration. Even though the maximum deviation between all computations discussed in this

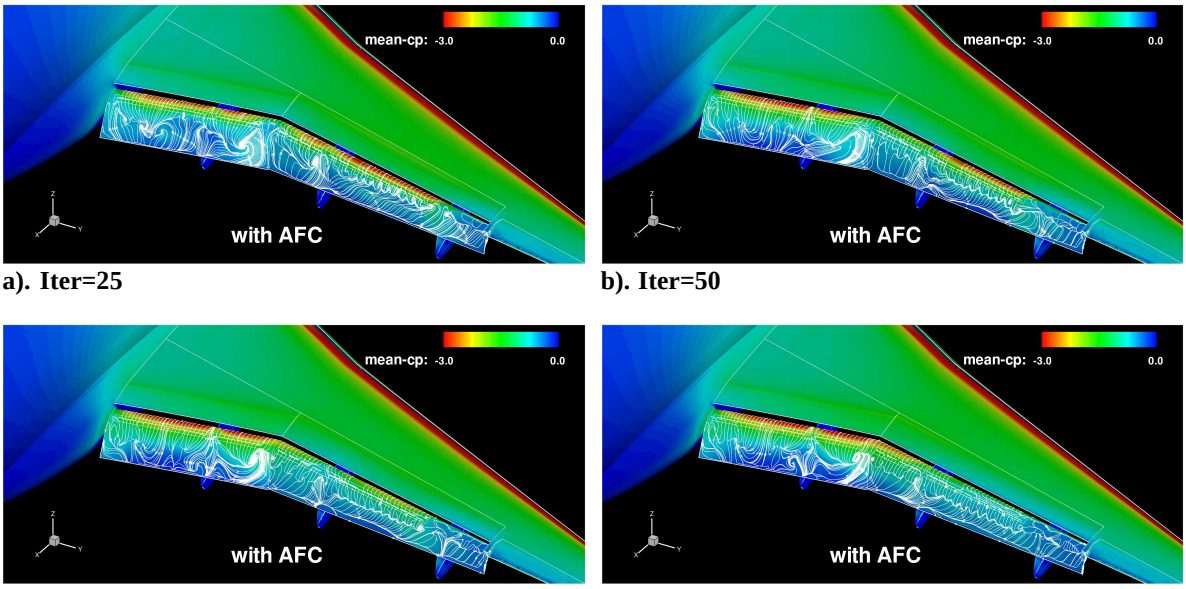

a). Iter=25 **b). Iter=50**

c). Iter=125 **d). Iter=250**

Figure 16. Flow topology with one AFC setup with different convergence level in the inner loop

chapter is lower 7 lift counts (1 lift count = 0.01), it is of relevance for the AFC application. For the discussed blowing momentum coefficient $C_\mu \approx 0.1\%$ such deviations represent ~ 25% of the lift gain by AFC. The evaluation of AFC capabilities is often analyzed through the lift enhancement and drag reduction by a specific blowing momentum and thus numerical errors of the order of ~25% should definitely be avoided. The exigent requirements trigger the numerical setup of *200* time steps for each actuation cycle and *125* inner iterations for all the simulations further addressed in this paper.

V. Computational Performance Studies for the AFC parameter C_μ

The analysis of the actuation setup with $C_\mu \approx 0.1\%$, $F^+=1$, DC=0.5 was already discussed in the previous chapter. This AFC setup shows a lift enhancement of 21 lift counts, in the linear lift regime, in comparison to the numerical results without AFC, while the large flow separation is significantly reduced by AFC, but not suppressed (Figure 17). The lift is evaluated as a result of the surface integration for the entire configuration. The pulsed blowing application on the flap has a global effect as shown in Figure 18. The pressure distributions at two wing sections, inboard, and outboard respectively, are the evidence of the global enhancement of AFC: higher suction peaks on the flap with a resulting lower pressure level for the main wing trailing edge and the further upstream effects, including the slat pressure distribution. The inboard section shows the suppression of the local flow separation, while in the outboard section only a local reduction through AFC is computed.

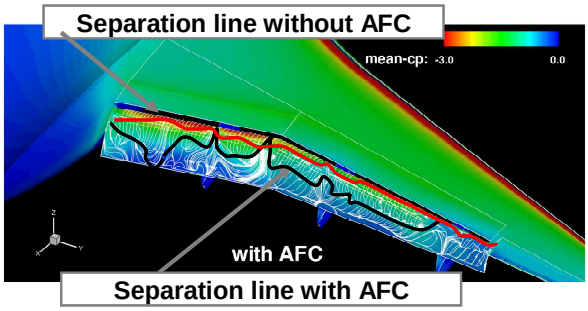

Figure 17. Separation lines on the flap with and without AFC (AFC: $C_\mu \approx 0.1\%$, $F^+=1$, DC=0.5)

The local change over time in the flow topology is shown in Figure 19 for the inboard section. The two instantaneous topologies correspond to the two stages of the pulsed blowing actuation, on and off, respectively. A local flow recirculation is present close to the flap trailing edge in the left view, at minimum lift, while the separation is vanished at the second time stage (right view, at maximum lift). The global lift coefficient varies up to 5 lift counts from the left- to the right- graph. The resulting coherent structures due to pulsed blowing are moving downstream without a major variation of the aerodynamic coefficients in time.

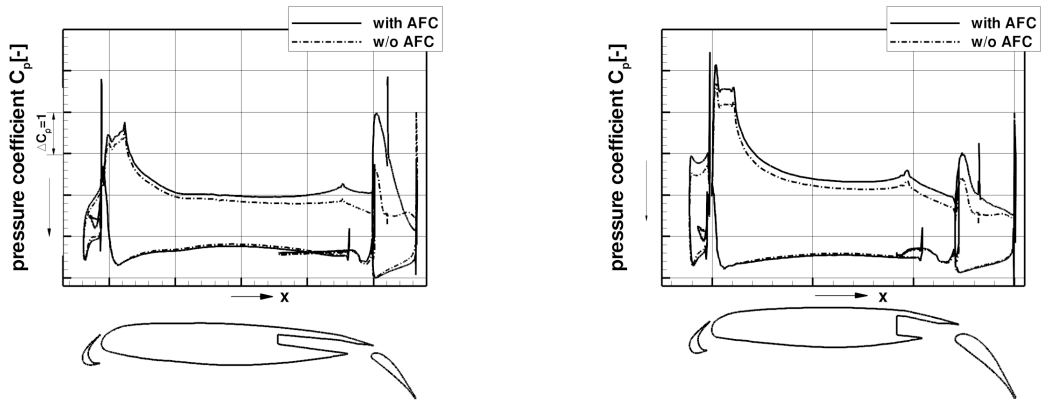

a). at y/b≈20% **b). at y/b≈42%**

Figure 18. Time-averaged pressure distributions for two wing sections

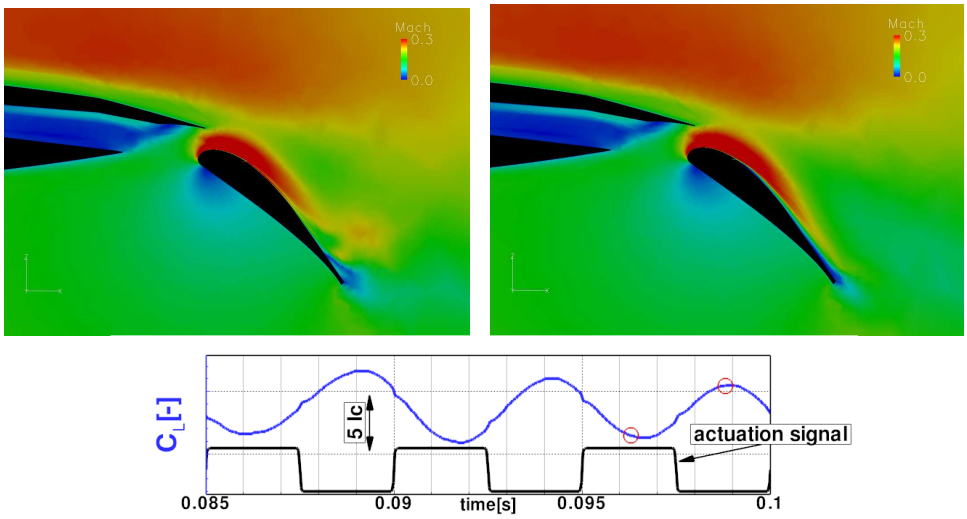

Figure 19. Local Mach number distributions in the inboard sections at two time stages (indicated by circles)

Figure 20 and Figure 21 depict the average surface pressure and average surfaces streamlines for the blowing momentum coefficients of $C_\mu \approx 0.2\%$, and $C_\mu \approx 0.4\%$, respectively. The results indicate lift increments of the order of up to 38 lift counts. The increase of momentum results in a reduction of the flow separation, and higher flap

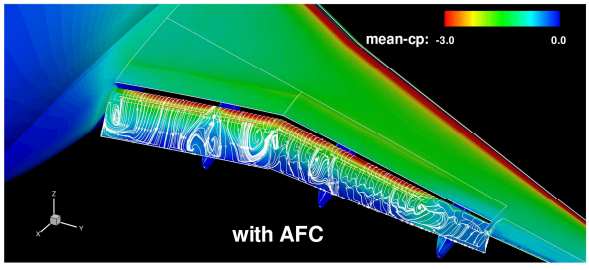

Figure 20. Flow topology and surface streamlines on the flap with AFC: $C_\mu \approx 0.2\%$, $F^+=1$, DC=0.5

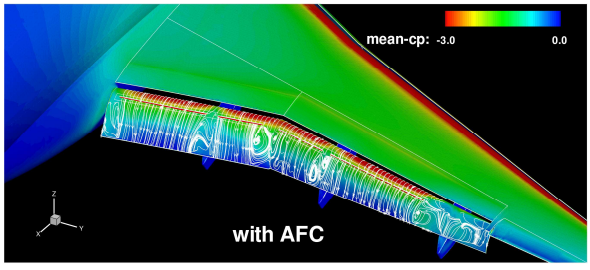

Figure 21. Flow topology and surface streamlines on the flap with AFC: $C_\mu \approx 0.4\%$, $F^+=1$, DC=0.5

suction peaks are computed. While for the inboard flap the flow is attached already downstream the actuators at $C_\mu \approx 0.2\%$, at the outboard flap the time-averaged flow shows no further separation only at $C_\mu \approx 0.4\%$. The portion of the outboard flap without actuators is always dominated by local flow separation. A benefit of the actuation is noticeable on the flap topology also outside the actuated regions. At the highest computed C_μ the extent of the separation in between the actuation regions is reduced in comparison to $C_\mu \approx 0.2\%$, for example near the flap track fairings.

We introduce here a remark on the time-dependent lift coefficient. A global and a local value are plotted over time in Figure 22. The global value coresponds to the complete aircraft configuration. The local value results after the integration of solely the flap's surface distribution. Locally, the peaks of C_L are associated with the end of the open-valve stages, while globally the maximum lift coresponds to the closed-valve stages. The phase shift is of the order of $0.7xc_{Flap}/U_\infty$ and is atributted to the time needed for the upstream elements to react on the change of circulation on the flap. Moreover, it becomes evident that the maximum changes in time for lift at $C_\mu \approx 0.2\%$ have the same order of magnitude as provided by the lower blowing momentum coefficient $C_\mu \approx 0.1\%$ (see also Figure 19).

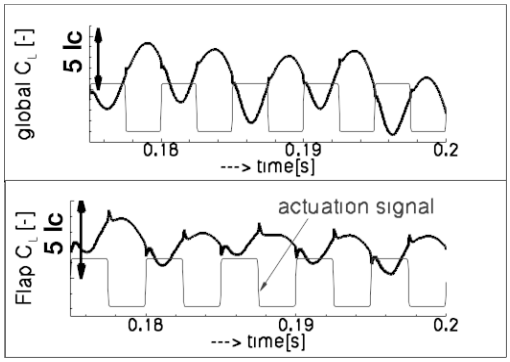

Figure 22. Global and local lift evolution over time with AFC: $C_\mu \approx 0.2\%$, $F^+=1$, DC=0.5

The active separation control on the flap shows a global enhancement of the aerodynamic lift coefficient with an increase of the resulting normal force for the constant angle of attack (Figure 23). The global increment is triggered by the actuation on the flap, and in the same time the surface distribution on the main wing is offering the highest increase for the normal force. The time-averaged data subscribe the typical multi-element aerodynamics effects as published by Smith[23]. He stated that an increased circulation of the downstream element causes the trailing edge of the adjacent upstream element to be in a region of high velocity. The increase of circulation on the flap results in a higher speed at the main-wing's trailing-edge which stretches up to its leading-edge, and so the speed at the trailing-edge of the slat is also increased. The successful separation suppression at moderate C_μ indicates that when separations occur this AFC technique is a beneficial solution. On the one side this technique might be applied

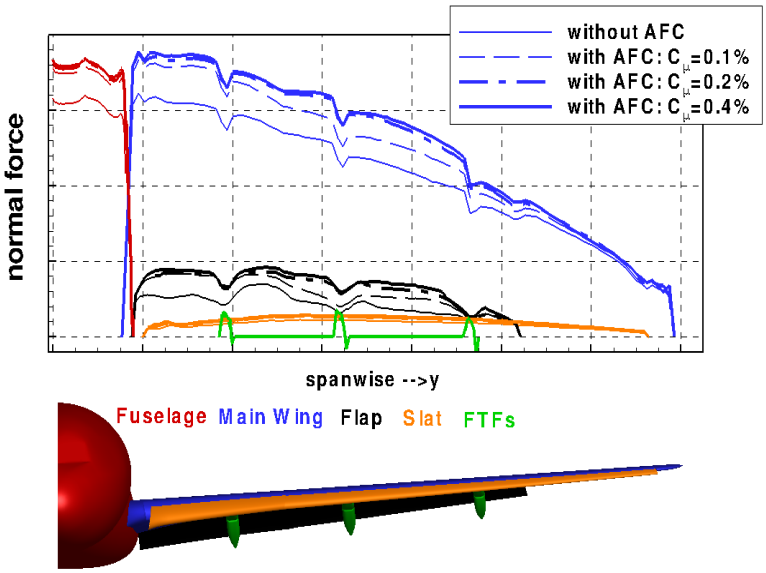

Figure 23. Overview of the time-averaged normal force distributions with and without AFC

towards replacing the multi-slotted flaps with single slotted-flaps. On the other side this AFC technique may serve for the treatment of local separations, for example at the wing-fuselage junction or downstream the slat's cut at the pylon location for under-wing mounted nacelles.

VI. Comparison of CFD Results with Experimental Findings

The purpose of this chapter is to provide a comparison of the numerical results with the experiments. The results are judged through the lift gain enhanced with the AFC application by means of time-averaged data. The numerical findings are calculated over several actuation cycles as discussed in the previous chapters, and compared with tunnel measurements of a six-component balance. In Figure 24 the lift coefficient is depicted for several blowing momentum coefficients at a fixed angle of attack. Both, experimental and numerical findings predict lift gains by AFC, with a steep increase for low values of C_μ and moderate increments for a higher C_μ. An overestimate of the lift gain is evident in the numerics. It has to be stated that the numerical approach uses an ideal square-shape signal at the actuation's slot-exit. However, the quality of actuation signal in the experiments was hampered by the limited available space for the instrumentation of the model. One may state that the numerical findings represent the ideal implementation of the present AFC technique for trailing-edge separation control. Taking this into account, the computed trends are of acceptable agreement with the experiments.

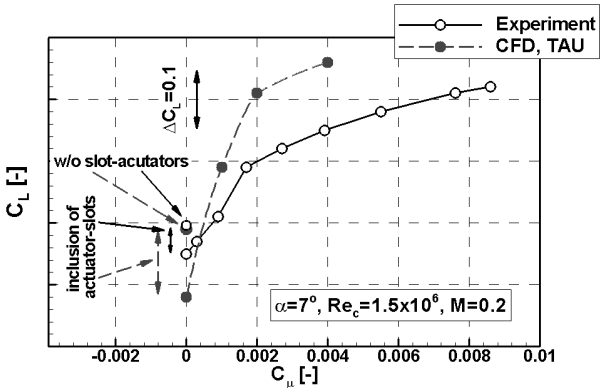

Figure 24. CFD versus Experiment: lift gain for different blowing momentum coefficients

The impact of including the actuator-slots was discussed in Part 1 of this paper with respect to the numerical results. The computed lift coefficient was about 6% lower with slots as without slots. It was stated that the lift loss is not solely triggered by the contribution of the slots integration. However, Figure 24 includes also the experimental and numerical results with and without slots for the baseline flow. The trend in the numerical results is again consistent with the experimental findings. Nevertheless, the selected numerical approach predicts a larger reduction of the lift coefficient due to the larger decrease of circulation on the trailing-edge flap. This has the disadvantage of deviating from measured baseline flow, but keeps the advantage of allowing the study of this AFC technique for slightly larger separations on the flap. Thus, the higher computed lift gains compared to the experiment result on a topology with a higher potential for the separation control, and depict that even at low energy consumption ($C_\mu \approx$ 0.1%), the aerodynamic enhancement can be significant (ΔC_L=0.21).

VII. Conclusions

Active flow separation control investigations were carried out for a 3D high-lift wing-body configuration under low speed atmospheric tunnel conditions. For a Mach number of *M=0.2* and Reynolds number of *Re=1.5x10^6* the experimental results confirm the concept for the pulsed blowing from the flap shoulder as a suitable tool for delaying or suppressing local flow separation with a remarkable global aerodynamic enhancement. The successful and unique experimental setup is a relevant subject for CFD analyses. The verification of the numerical investigations points out that large computational times are required for a consistent evaluation of the unsteady flow. It is highlighted that the URANS AFC simulations are feasible with the compressible solver DLR-TAU-Code. The numerical results are of acceptable agreement in comparison with the experimental findings and offer us viable details of the flow topologies. The changes for the aerodynamic coefficients over time do not show an extreme variation, e.g. maximum 5 lift counts for the lift coefficient when AFC is applied. The global lift enhancement is mainly triggered by increments in the main wing surface distribution as result of the improved circulation at the trailing edge flap. The flow patterns at different blowing momentum coefficients indicate that a further optimization of the energy consumption may be achieved. The inboard flap shows the local separation suppression for $C_\mu \approx$ 0.2%, while only at $C_\mu \approx$ 0.4% a fully attached flow is computed for the outboard flap. At the highest investigated blowing momentum, $C_\mu \approx$ 0.4%, the lift gain is estimated at ΔC_L=0.38, while for a C_μ of only 0.1 % a gain of 21 lift counts was computed. In direct comparison with the experimental findings the numerical results show overestimated lift

gains for fixed blowing momentum coefficients. These results are consistent since the limitations of the tunnel testing remarkably disturbed the targeted actuation's square-shape signals at high frequency and are considered as the main trigger for lower lift increments in the experiments. However, the trends are in reasonable agreement between the numerical- and experimental- findings. A further strategy to better use the available methods may be to verify the impact of the "disturbed" jet velocity profiles by means of URANS simulations.

Nevertheless, all aerodynamic investigations have been conducted for a unique high-lift model with a comparatively high-complexity. Both the experimental and the numerical application will contribute to the further development of this AFC technique.

Acknowledgments

The experimental data[24] were provided in the present form with special permission by Airbus, in order to compare with the numerical results. The authors would like to thank Airbus and TU Berlin for the help and ongoing support.

References

[1]Rudolph, P.K.C., "High-Lift Systems on Commercial Subsonic Airliners," NASA CR 4746, Sept. 1996.

[2]Schlichting, H., *Grenzschicht-Theorie*, 5th edition, Verlag G. Braun, vol. 5, no. 1, 2001, pp. 27-33.

[3]Tinapp, F. and Nitsche, W., "LDV-Measurements on a High-Lift Configuration with Separation Control," *Proceedings of the 9th International Symposium on Applications of Laser Techniques to Fluid Dynamics*, Lisbon, Portugal, 1998, pp. 19.1-19.8.

[4]Tinapp, F. and Nitsche,W., "On Active Control of High-Lift Flow," *Engineering Turbulence Modeling and Experiments* edited by W. Rodi and D. Laurence, 4. Elsevier Publ., Amsterdam, 1999, pp. 619-626.

[5]Tinapp, F. and Nitsche, W., "Separation Control on a High-Lift Configuration by Periodic Excitation," *New Results in Numerical and Experimental Fluid Mechanics III*, Vol.77, Springer Verlag, Heidelberg, 2002.

[6]Petz, R. and Nitsche, W., "Active Separation Control on a High-Lift Configuration by a Periodically Pulsating Jet," ICAS 2004-118, Yokohama, Japan, 2004.

[7] Petz, R. and Nitsche, W., "Active Separation Control on the Flap of a Two-Dimensional Generic High-Lift Configuration," *Journal of Aircraft* , Vol. 44, No. 3, 2007, pp. 865-874.

[8]Petz, R., "Aerodynamic Benefits of Pulsed Blowing Applied to High-Lift Airfoils," *Proceedings of First CEAS European Air and Space Conference*, Berlin, 2007.

[9]Becker, R., King, R., Petz, R. and Nitsche, W., "Adaptive Closed-Loop Separation Control on a High-Lift Configuration Using Extremum Seeking," *Journal of Aircraft*, Vol. 44, No. 3, 2007, pp. 865-874.

[10]Haucke, F., Peltzer, I. and Nitsche,W., "Active Separation Control on a Slatless 2D High-Lift Wing Section," *Proceedings of the 26th ICAS Congress*, ICAS-2008-175, 2008.

[11]Wild, J., Wichmann, G., Haucke, F., Peltzer, I. and Scholz, P., "Large scale separation flow control experiments within the German Flow Control Network," *47th AIAA Aerospace Sciences Meeting*, AIAA Paper 2009-530, Jan. 2009.

[12]Naveh, T., Seifert, A., Tumin, A., and Wygnanski, I., "Sweep effect on the parameters governing the control of separation by periodic excitation," *Journal of Aircraft* , Vol. 35, No. 3, 1998, pp. 510-512

[13]Joslin, R.D., Miller, D.N., "Fundamentals and Applications of Modern Active Flow Control", *AIAA Book, Progress in Astronautics and Aeronautics* , Vol. 231, ISBN 978-1-56347-983-0, 2009

[14]Seifert, A., Bachar, T., Koss, D., Shepshelovich, M., and Wygnanski, I., "Oscillatory blowing, a tool to delay boundary layer separation," *AIAA Journal*, Vol. 31, No. 11, 1993, pp. 2052–2060.

[15]Bauer, M., Peltzer, I., Nitsche, B., and Goelling, B., „Active Flow Control on an Industry-Relevant Civil Aircraft Half Model", Vol. 108 of *Notes on Numerical Fluid Mechanics and Multidisciplinary Design*, Springer Verlag, 2010, pp. 95-107.

[16]http://centaursoft.com, May 2010.

[17]Gerhold, T., "Overview of the Hybrid RANS Code TAU," *MEGAFLOW - Numerical Flow Simulation for Aircraft Design*, Vol. 89 of *Notes on Numerical Fluid Mechanics and Multidisciplinary Design*, Springer Verlag, 2005, pp. 81-92.

[18]Menter, F. R., "Two-Equation Eddy-Viscosity Turbulence Models for Engineering Applications," *AIAA Journal*, Vol. 32, No. 8, 1994, pp. 1598-1605.

[19]Rudnik, R., "Evaluation of the Performance of Two-Equation Turbulence Models for Airfoil Flows," Ph.D. Dissertation, Transportation and Applied Mechanics Dept. , Technical University Berlin, Germany, 1997.

[20]Knopp, T., "The actuation boundary condition for flow control in the DLR TAU Code," DLR Report, IB-Nr. 224 – 2010 A44, Germany, 2010.

[21]Togiti, V., Ciobaca, V., Eisfeld, B. and Knopp, T., "Numerical Simulation of Steady Blowing Active Flow Control Using a Differential Reynolds Stress Model," *CEAS/KATnet II Conference on Key Aerodynamics Technologies*, Bremen, Germany, May 2009.

[22]Ciobaca, V., "Parameter study for a slatless 2D high-lift airfoil with active separation control using a URANS approach," *Notes on Numerical Fluid Mechanics and Multidisciplinary Design*, Springer Verlag (to be published).

[23]Smith, A.M.O., "High-Lift Aerodynamics", *AIAA 6th Aircraft Design, Flight Test and Operation Meeting*, 1974

[24]Goelling, B. and Bieler, H., "High lift Active flow control investigations in National R&T projects," *CEAS/KATnet II Conference on Key Aerodynamics Technologies*, Bremen, Germany, May 2009.